Journal of Microscopy, *Vol.* 133, *Pt* 1, *January* 1984, *pp.* 27–39.
Received 1 *November* 1982; *accepted* 29 *March* 1983

Differential phase contrast in scanning optical microscopy

by D. K. HAMILTON *and* C. J. R. SHEPPARD, *University of Oxford, Department of Engineering Science, Parks Road, Oxford OX*1 *3PJ*

KEY WORDS. Scanning optical microscopy, differential interference contrast, Nomarski optics, laser, biological specimens, image formation, high resolution, optical microscopy.

SUMMARY

High-quality high-resolution transmission and reflection images produced using a scanning optical microscope and the split-detector technique are presented. These images exhibit differential phase contrast, the method avoiding some drawbacks of the usual Nomarski DIC arrangement. Imaging is treated theoretically and compared with the Nomarski method.

1. INTRODUCTION

Although Nomarski differential interference contrast (Nomarski, 1955) has become a widely used and powerful technique in optical microscopy it does have a number of disadvantages. A compromise must be made between contrast and signal level so that for objects with weak variations the signal may be very weak and in order to obtain adequate contrast the condenser must often be stepped down somewhat so that optimum resolution is no longer achieved. In general the image is formed by a complicated mixture of different contrast mechanisms including non-differential amplitude and differential amplitude contrast and with birefringent specimens it must be used with care.

A method widely used for scanning transmission electron microscopy (Dekkers & de Lang, 1974, 1977) based on a split detector, overcomes these problems, and indeed its use in scanning optical microscopy was suggested in the paper in which it was originally described (Dekkers & de Lang, 1974). However, until now, production of high-quality high-resolution optical images using the technique has not been reported.

A laser beam is focused to a fine spot on the specimen and the light either transmitted through, or reflected from, the object is incident on a large area photodetector consisting of two semicircular elements (Fig. 1). In the absence of a phase gradient in the object each semicircle gives the same signal so that their difference is zero, but the presence of a phase gradient deflects the transmitted beam so that one half of the detector has a larger output than the other. For weak phase gradients the difference signal is proportional to the phase gradient. An image is built up by mechanically scanning the object relative to the laser beam, and using the difference signal to modulate the brightness of a CRT display scanned in synchronism with the object as in the usual arrangement of the scanning optical microscope (Sheppard, 1980a). If alternatively the sum of the two detector elements is formed, a non-differential amplitude contrast image results. The two detector elements if used individually produce a non-differential amplitude contrast image with either positive or negative differential phase contrast superimposed.

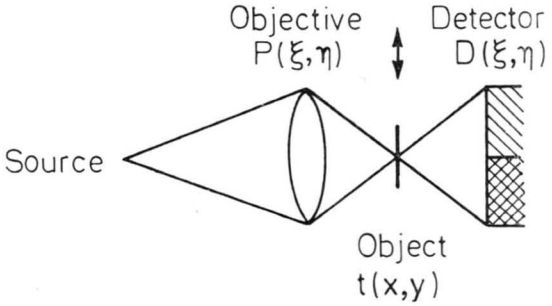

Fig. 1. Schematic diagram of a transmission-mode scanning optical microscope with large area detector, sensitivity distribution $D(\zeta, \eta)$.

2. EXPERIMENTAL WORK

A range of objects has been observed using a scanning optical microscope in both reflection and transmission modes. The detector was formed by a silicon solar cell, cut into halves, each part being fed into a preamplifier specially designed to give low noise and the necessary bandwidth in combination with the large source capacitance presented by the detectors. Small corrections for imbalance between the detectors could be made by varying the amplifier gains slightly. The subsequent circuit was arranged so that either of the two signals separately, their

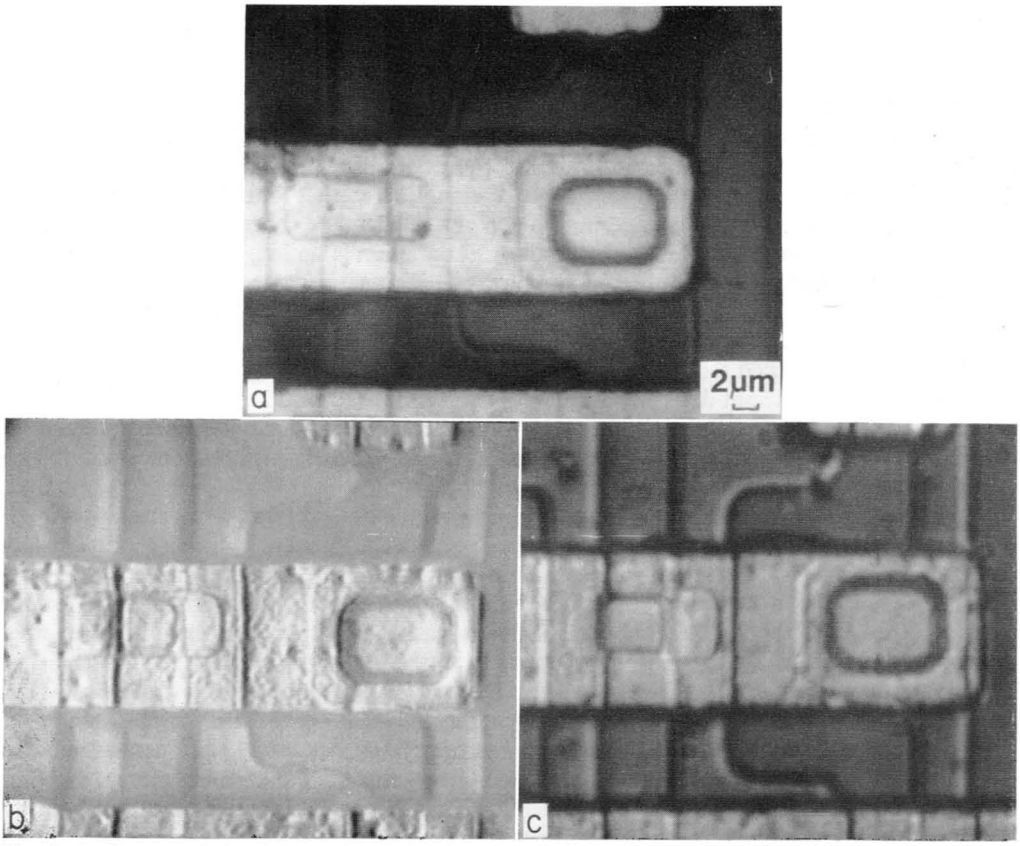

Fig. 2. An integrated circuit viewed in reflection: (a) amplitude image, (b) differential phase image, (c) a similar region viewed in a Zeiss microscope using Nomarski DIC.

sum, or their difference could be displayed on the cathode ray tube. As the difference signal is bidirectional, a constant voltage had to be added to it such that zero difference signal gave approximately half full screen brightness. The microscope employed a HeNe laser ($\lambda = 0{\cdot}6328$ μm).

For the reflection experiments an objective with a numerical aperture of 0·85 was used. Here the reflected light travelled back through the objective which thus formed the collector lens and this, analogous to the condenser in a conventional microscope, was therefore filled. Figure 2 shows high magnification reflection images from part of an integrated circuit. Figure 2(a) is the image formed by adding the signals from the detector halves, and is identical to a conventional image; the bright regions of this image correspond to metallization which stands up above the silicon surface. Figure 2(b) shows the differential phase image formed by subtracting the two detector signals. (Positive or negative contrast may be formed according to which signal

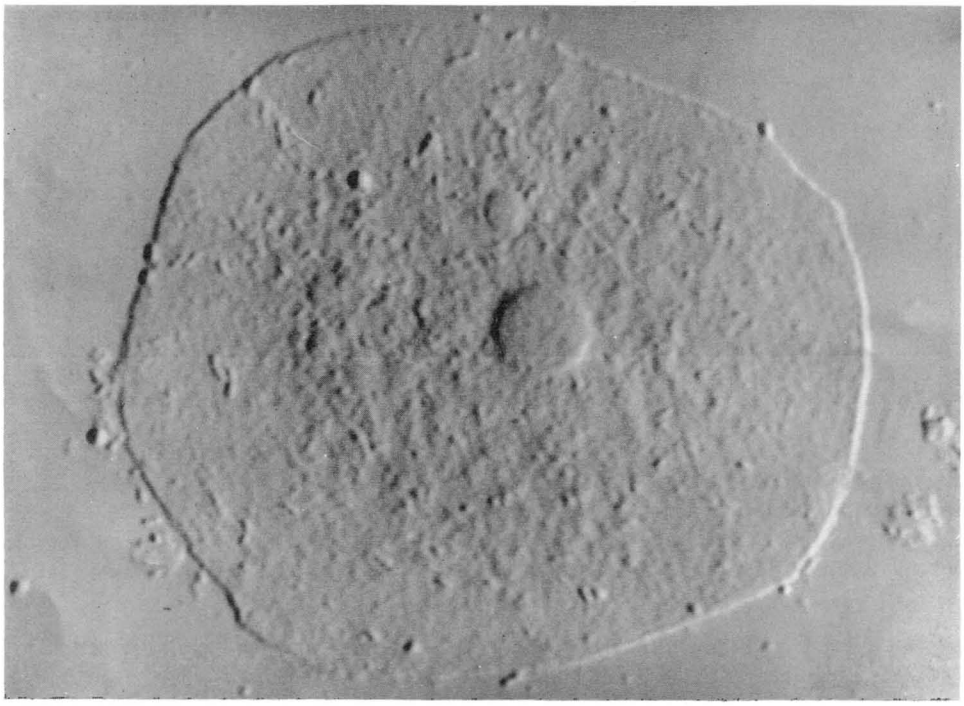

Fig. 3. An unstained buccal epithelium cell in transmission using light from an HeNe laser (λ=633 nm) and an objective of numerical aperture 0·5.

is used as subtrahend.) This image shows a pronounced effect of relief and considerable detail, due to small changes in surface height, particularly on the surface of the metallization. The image from just one half of the detector consists of a conventional image with differential phase contrast superimposed, again leading to an impression of relief. Figure 2(c) records, for comparison, a similar region viewed in a Zeiss microscope, again with an objective of numerical aperture 0·85, but using the Nomarski DIC method.

Figures 3 and 4 show buccal epithelium cells in transmission, using the split detector technique to differentiate in the horizontal direction. The specimens were unstained so that a conventional image formed by adding the detector outputs showed no observable detail.

3. THEORY OF IMAGE FORMATION

Pure differential phase contrast gives an image whose intensity is proportional to the rate of

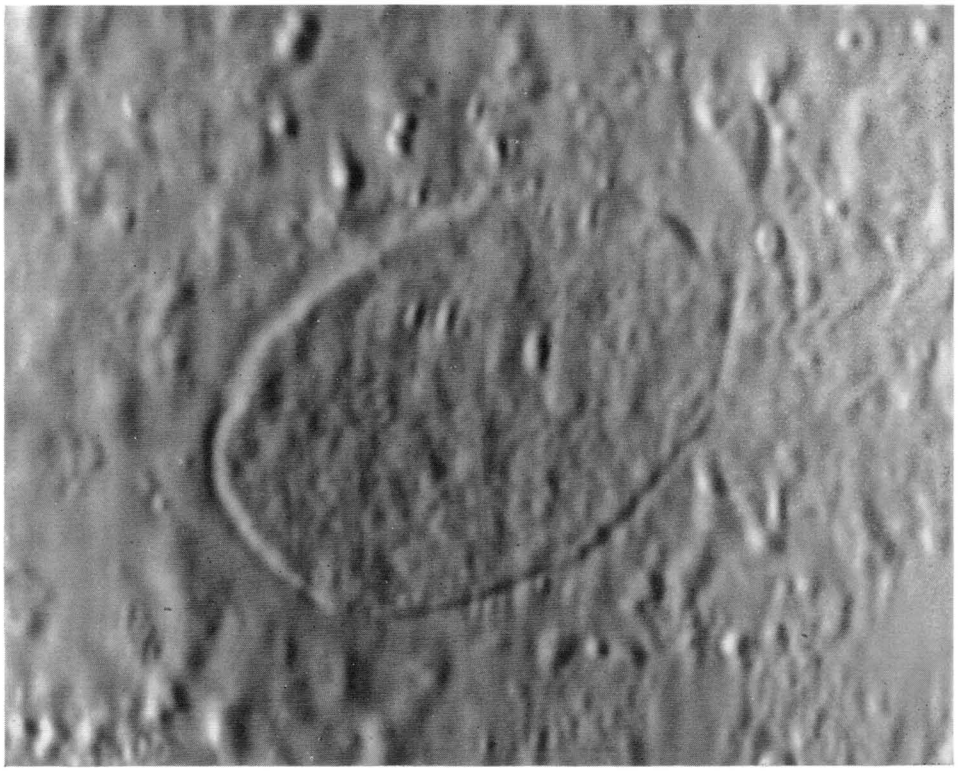

Fig. 4. The nucleus of a different buccal epithelium cell in transmission using light from an HeCd laser (λ=440 nm), an oil-immersion objective of numerical aperture 1·3 and a detector of numerical aperture 0·92.

change of phase across the object modulated by the intensity of the light transmitted. The split detector method results in imaging which approximates to this ideal.

A scanning microscope with arbitrary detector distribution (Fig. 1) behaves as a partially coherent system so that the image intensity may be written (Sheppard & Choudhury, 1977)

$$I(x,y)=\int\int\int\int_{-\infty}^{+\infty} C(m,n;p,q)\,T(m,n)\,T^{\star}(p,q)\exp\{-2\pi j[(m-p)x+(n-q)y]\}\,\mathrm{d}m\,\mathrm{d}n\,\mathrm{d}p\,\mathrm{d}q \quad (1)$$

where $C(m,n;p,q)$ is the partially coherent transfer function, which is a property of the optical system only, and $T(m,n)$ is the spectrum of the object amplitude transmittance given by its Fourier transform

$$T(m,n)=\int\int t(x,y)\exp[2\pi j(mx+ny)]\,\mathrm{d}x\,\mathrm{d}y. \quad (2)$$

The transfer function is given by (Sheppard & Choudhury, 1977)

$$C(m,n;p,q)=\int\int_{-\infty}^{+\infty} P(\xi-\tilde{m},\eta-\tilde{n})P^{\star}(\xi-\tilde{p},\eta-\tilde{q})\,D(\xi,y)\,\mathrm{d}\xi\,\mathrm{d}\eta \quad (3)$$

in which $P(\xi,\eta)$ is the pupil function of the objective, expressed as a function of normalized coordinates ξ,η such that

$$P(\xi,\eta)=0;\ (\xi^2+\eta^2)^{1/2}>1 \quad (4)$$

$D(\xi, \eta)$ is the detector sensitivity distribution, and $\tilde{m}, \tilde{n}; \tilde{p}, \tilde{q}$ are normalized spatial frequencies

$$\tilde{m} = m\lambda/2 \sin \alpha \tag{5}$$

and so on, with wavelength λ and numerical aperture sin α.

For line structures such that the object transmittance is a function of x only the image is

$$I(x) = \int_{-\infty}^{+\infty}\int C(m; p)\ T(m)\ T^{\star}(p) \exp\ [-2\pi j(m-p)x]\ \mathrm{d}m\, \mathrm{d}p \tag{6}$$

with

$$C(m; p) = \int_{-\infty}^{+\infty}\int P(\xi - \tilde{m}, \eta) P^{\star}(\xi - \tilde{p}, \eta)\ D(\xi, \eta)\ \mathrm{d}\xi\, \mathrm{d}\eta. \tag{7}$$

For the case of the split detector the transfer function is evaluated by subtracting integrals over semicircles and displaced circles. For an aberration-free system the partially coherent

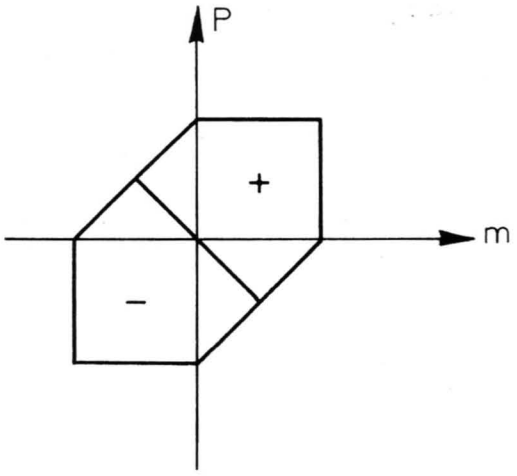

Fig. 5. Symmetry of the transfer function for differential phase contrast.

transfer function obeys the symmetry shown in Fig. 5, which applies for pure differential phase contrast (Wilson & Sheppard, 1980), its value being given for m and p of the same sign

$$C(m; p) = \{\Lambda(\tilde{m}) - \Lambda(2\tilde{m})\} \operatorname{sgn}(\tilde{m});\ |\tilde{m}| > |\tilde{p}| \tag{8}$$

where $\Lambda(\tilde{m})$ is the convolution between two circles

$$\left.\begin{aligned} \Lambda(\tilde{m}) &= \frac{2}{\pi}\left\{\cos^{-1}|\tilde{m}| - |\tilde{m}|\sqrt{1-\tilde{m}^2}\right\};\ |\tilde{m}| < 1 \\ &= 0 \qquad\qquad\qquad\qquad\quad ;\ |\tilde{m}| > 1 \end{aligned}\right\}. \tag{9}$$

and sgn $(\tilde{m})$ is the signum function

$$\left.\begin{aligned} \operatorname{sgn}(\tilde{m}) &= 1;\ \tilde{m} > 0 \\ &= -1;\ \tilde{m} < 0 \end{aligned}\right\}. \tag{10}$$

For m and p of opposite sign we have

$$C(m; p) = \{\Lambda(\tilde{m} - \tilde{p}) - \Lambda(2\tilde{m})\} \operatorname{sgn} m;\ |\tilde{m}| > |\tilde{p}|. \tag{11}$$

For a weak object of the form

$$t(x)=1+t_1(x)$$

with $|t_1(x)|$ small, the cross-product terms in T_1 in equation (6) are negligible leaving

$$I(x)=C(0;0)+2\mathrm{Re}\left\{\int_{-\infty}^{+\infty} C(m;0)\ T_1(m)\exp(-2\pi jmx)\,\mathrm{d}m\right\}. \tag{13}$$

For a weak object amplitude variations result in a real t_1 whereas phase variations result in an imaginary t_1. It can be shown that (Wilson & Sheppard, 1980; Sheppard & Wilson, 1980) if $C(m;0)$ is real and even non-differential amplitude contrast results, if it is real and odd differential phase contrast is formed, if it is imaginary and even we have non-differential phase contrast, whereas if it is imaginary and odd we have differential amplitude contrast. The imaging for weak line objects is described completely by the weak object transfer function

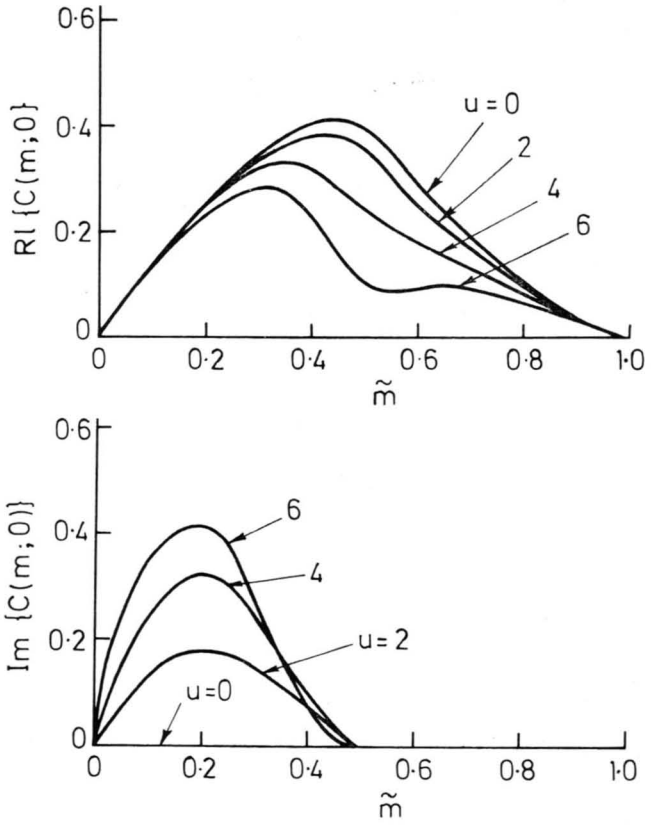

Fig. 6. The weak object transfer function for a split-detector system with defocus.

$C(m;0)$. This is generally true, regardless of the degree of partial coherence in the imaging system, which thus degenerates to a linear system. For the split-detector configuration $C(m;0)$ is real and odd (Fig. 6) for an aberration-free system, resulting in pure differential phase contrast. If, on the other hand, the system is defocused by an axial distance z, resulting in a pupil function

$$P[(\xi^2+\eta^2)^{1/2}]=\exp\left[\tfrac{1}{2}ju\,(\xi^2+\eta^2)\right],\ (\xi^2+\eta^2)^{1/2}<1. \tag{14}$$

where u is the optical coordinate

$$u = kz \sin^2 \alpha. \tag{15}$$

the weak object transfer function is complex with a real part

$$\left.\begin{aligned} C_R(m;0) &= \frac{4}{\pi}\int_0^{\tilde{m}} \cos(2um\xi)\left\{1-(\xi+\tilde{m})^2\right\}^{1/2} \mathrm{d}\xi, \ \tilde{m} \leqslant 0{\cdot}5 \\ &= \frac{4}{\pi}\int_0^{1-\tilde{m}} \cos(2u\tilde{m}\xi)\left\{1-(\xi+m)^2\right\}^{1/2} \mathrm{d}\xi, \ 0{\cdot}5 \leqslant \tilde{m} \leqslant 1 \\ &= 0 \qquad\qquad\qquad\qquad\qquad\qquad\qquad\qquad\qquad\qquad , \ \tilde{m} > 1 \end{aligned}\right\} \tag{16}$$

and an imaginary part

$$\left.\begin{aligned} C_I(m;0) &= \frac{4}{\pi}\int_{\tilde{m}}^{1-\tilde{m}} \sin(2u\tilde{m}\xi)\left\{1-(\xi+\tilde{m})^2\right\}^{1/2} \mathrm{d}\xi, \ \tilde{m} \leqslant 0{\cdot}5 \\ &= 0 \qquad\qquad\qquad\qquad\qquad\qquad\qquad\qquad\qquad\qquad , \ \tilde{m} > 0{\cdot}5 \end{aligned}\right\}. \tag{17}$$

These also are shown in Fig. 6. The imaginary part results in differential amplitude contrast. The transfer function $C(0;0)$ is zero so that in order that the image intensity is always positive an offset of $1/2$ must be added. The curves of Fig. 6 are well behaved, without many sign changes.

4. CALCULATION OF IMAGES OF IDEAL OBJECTS

The image of a weak phase line of strength a_i can be calculated as the Fourier transform of the transfer function $C(m;0)$. For an unaberrated system we obtain (Ditkin & Prudnikov, 1965), ignoring a constant factor,

$$\Delta I(v) = 2a_i\{\mathcal{J}_0(v/2) + \mathcal{J}_2(v/2) - \mathcal{J}_0(v) - \mathcal{J}_2(v)\}/v \tag{18}$$

where v is the optical coordinate

$$v = kr \sin \alpha \tag{19}$$

and $\mathcal{J}_n$ is a Bessel function of order n.

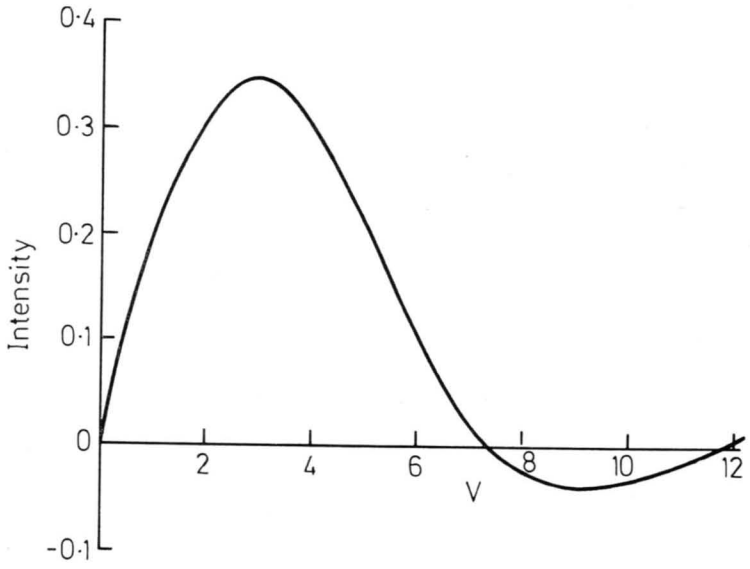

Fig. 7. The image of a weak line object in differential phase contrast.

Using the usual recurrence relationship this may be written

$$\Delta I(v)=4a_i\{2\mathcal{J}_1(v/2)-\mathcal{J}_1(v)\}/v \tag{20}$$

and is shown in Fig. 7. The intensity variation is purely real, but is allowed to be negative as it is superimposed on a constant offset.

The image of a weak phase edge with phase difference δ may be calculated by integrating equation (18) to obtain

$$\begin{aligned}\Delta I(v)&=\delta\left[\ln 2-\frac{1}{2}\left\{\frac{2\mathcal{J}_1(v/2)}{v/2}-\frac{2\mathcal{J}_1(v)}{v}\right\}-\int_{v/2}^{v}\frac{\{1-\mathcal{J}_0(v)\}}{v}\,\mathrm{d}v\right]\\&=\delta\left[\ln 2-\frac{1}{2}\left\{\mathcal{J}_0(v/2)-\mathcal{J}_2(v/2)-\mathcal{J}_0(v)+\mathcal{J}_2(v)\right\}-\int_{v/2}^{v}\frac{\{1-\mathcal{J}_0(v)\}}{v}\,\mathrm{d}v\right]\end{aligned} \tag{21}$$

which is shown in Fig. 8.

Turning now to a weak point object of strength a, the image is most easily calculated directly as

$$I(v,\theta)=\int_0^{2\pi}\int_0^{\infty}|P_1(\rho)+ah_1(v)\exp[j\rho v\cos(\theta-\phi)]|^2\,D(\rho,\phi)\,\rho\,d\rho\,d\phi \tag{22}$$

where

$$\rho^2=\xi^2+\eta^2 \tag{23}$$

and

$$h_1(v)=\frac{2\mathcal{J}_1(v)}{v} \tag{24}$$

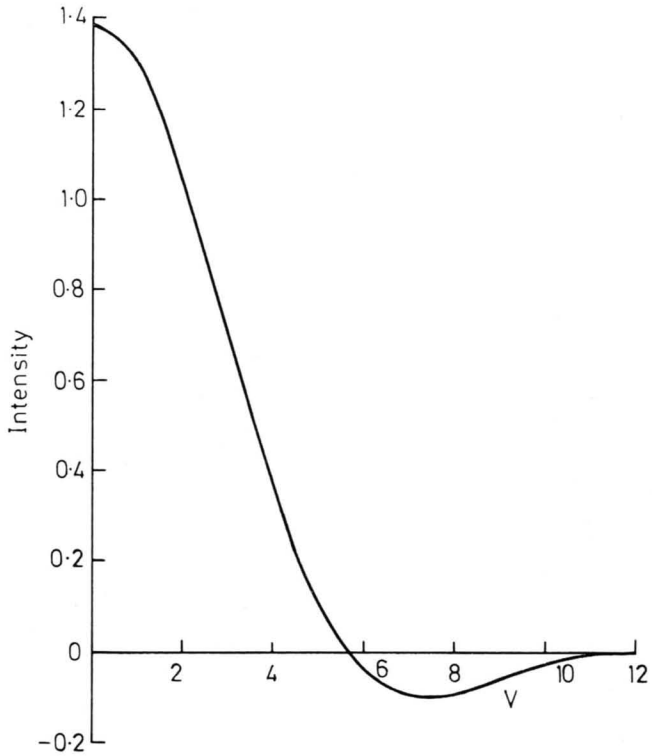

Fig. 8. The image of a weak phase edge in differential phase contrast.

is the amplitude point spread function of the objective. If a is small the image for the split detector case is

$$I(v, \theta)=4a_i\left(\frac{2\mathfrak{J}_1(v)}{v}\right)\int_0^{\pi}\int_0^{1}\sin\{v\rho\cos(\theta-\phi)\}\,\rho d\rho d\phi \tag{25}$$

where a_i is the imaginary part of a. In general this may be evaluated in terms of incomplete Bessel and Struve functions (Barna, 1977), but for $\theta=\pi/2$ we obtain

$$I(v)=\frac{2\mathfrak{J}_1(v)}{v}\times\frac{2H_1(v)}{v} \tag{26}$$

in which H_1 is a Struve function of order unity, and this is shown in Fig. 9. It should be noted that the angular dependence of the weak point spread function is rather complicated, although it does not depart greatly from the ideal behaviour.

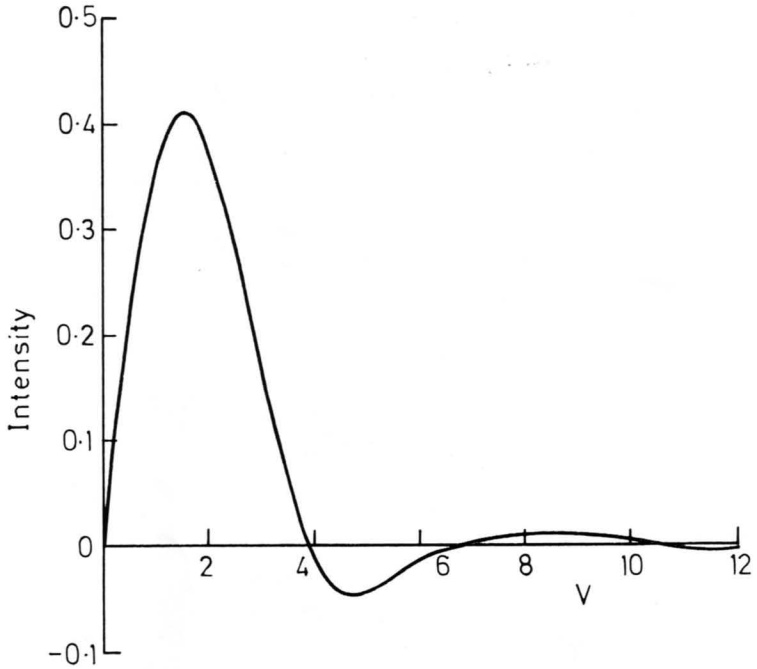

Fig. 9. The image of a weak point object in differential phase contrast in the direction of differentiation.

Turning now to strong objects it is seen that the image of a strong point object with the split detector is always zero. A point object produces an image only through interference with other radiation. For example, two point objects produce no image if they are well separated or coincident, but when slightly separated an image is formed. For a strong phase edge, with phase difference δ, the spectrum may be written

$$T(m)=\cos(\delta/2)\,\delta(m)+\sin(\delta/2)/\pi m \tag{27}$$

By considering the symmetry of $C(m; p)$ for the split detector case we find that the only contributions to the image are from the cross-product terms so that equation (21) is still valid with δ replaced by sin δ. The shape of the phase edge image is not dependent on the magnitude of the phase change, contrary to the results from conventional or confocal microscopes. One of the

most important properties of a differential phase contrast microscope is its response to a phase gradient. Consider an object with

$$t(x)=\exp(j\phi' x) \tag{28}$$

where ϕ' is the phase gradient. We thus have

$$T(m)=\delta(m-\phi'/2\pi) \tag{29}$$

which contains only one spatial frequency component. The image of the phase gradient is thus (Sheppard, 1980b)

$$I(x)=C(\phi'/2\pi;\ \phi'/2\pi) \tag{30}$$

that is it is independent of position and completely specified by $C(m; m)$. From equation (3) this is independent of aberrations or defocus. For the split detector case it is equal to the aberration-free $C(m; 0)$. If the phase gradient changes only slowly compared with the spread function the image intensity variation can be determined from equation (30). Thus for a monotonic phase (or height) variation the intensity first of all either increases or decreases according to the direction of phase change. If the maximum gradient in a monotonic phase step is quite small a bright or dark line appears in the image. If, on the other hand, the maximum

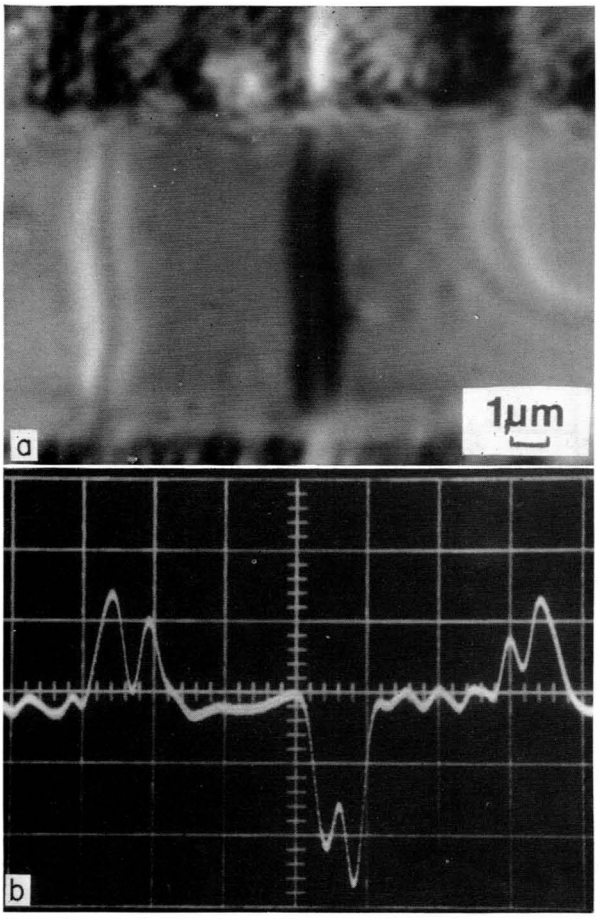

Fig. 10. Differential phase image of a surface with smoothly varying height, showing double fringes: (a) image, (b) line scan.

gradient is such that the intensity goes over the maximum of the curve shown in Fig. 6, the image consists of two fringes. This is demonstrated in Fig. 10, in which the microscope was focused on to the silicon surface.

5. COMPARISON WITH NOMARSKI DIFFERENTIAL INTERFERENCE CONTRAST

The images produced using the split detector technique bear some similarities with those formed using Nomarski differential interference contast, but there are also important differences. In the Nomarski method a polarizer produces a plane polarized wave, which is then split into two slightly spatially separated beams polarized orthogonally with respect to each other. After traversing the condenser, object and objective the beams are recombined spatially with a compensator, which is also used to adjust the relative phase between the two beams. The beams are then mixed using an analyser to form an image. The polarizer and analyser are adjusted to extinction when there is no phase gradient in the object. With an object which introduces both a change in amplitude and phase between the two beams the resultant intensity is

$$I=|(t+t'\Delta)-t|^2 \tag{31}$$

$$=|t'|^2\Delta^2 \tag{32}$$

where t' is the derivative of the object amplitude transmittance and Δ is the beam separation in the object. This represents what has been termed 'differential contrast'—both amplitude and phase variations are imaged in a non-linear manner, and the system has similarities in common with dark-field imaging. The phasors representing the various beams are shown in Figs. 11(a) and 11(b), the resultant amplitude being labelled r.

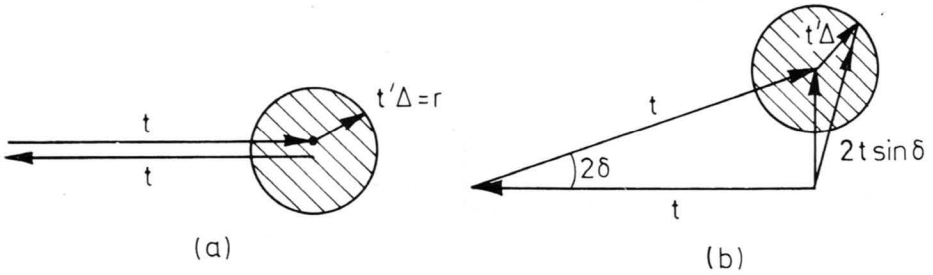

Fig. 11. Signal r in the Nomarski DIC microscope: (a) at extinction, (b) with compensator set to give bias angle of 2δ.

In order to produce linear imaging of small phase variations the compensator is used to introduce a further small phase difference 2δ between the two beams (Fig. 11b). The phasor $2t \sin \delta$ is approximately in quadrature with t so that providing δ is small and

$$t'\Delta \ll 2t \sin \delta \tag{33}$$

the resultant intensity

$$I=|r|^2=4t^2\{\sin^2\delta-\theta'\Delta \sin \delta \cos \delta\} \tag{34}$$

depends only on the phase gradient in the object and not the amplitude gradient. The image intensity consists of positive or negative variations about a mean level given by the well-known sine squared law, the variations being proportional to the phase gradient in the object.

So far we have neglected diffraction effects but these can be incorporated by replacing $T(m)$ in equation (1) by the sum of the two components from the two beams

$$T(m)\rightarrow[\exp(-2j\delta)\exp(-2\pi jm\Delta)-1]\,T(m) \tag{35}$$

the exponential term in m representing the spatial shift of the second beam. We thus obtain for the effective transfer function

$$C_{\text{eff}}(m;p)=[\exp(-2j\delta)\exp(-2\pi jm\Delta)-1][\exp(2j\delta)\exp(2\pi jp\Delta)-1]\,C(m;p) \quad (36)$$

or if Δ is small,

$$C_{\text{eff}}(m;p)\approx 4\{\sin^2\delta-\pi\Delta(m+p)\sin\delta\cos\delta+j\pi\Delta(m-p)\sin^2\delta\}C(m;p) \quad (37)$$

where $C(m;p)$ is the transfer function of the system without splitting the beam. The effective transfer function is thus made up of the sum of three components, the first representing non-differential amplitude imaging, the second the required differential phase contrast and the third differential amplitude contrast. There are, in addition, higher order terms in Δ representing non-linear components and non-differential phase contrast. The strengths of the various components depend on the compensation, decreasing δ decreasing the strength of the differential phase contrast component but increasing its contrast relative to the background.

Let us consider the imaging of an object consisting of a constant phase gradient, ϕ'. Then the image intensity is given by equation (30) to be $C(m;m)$ with

$$m=\phi'/2\pi. \quad (38)$$

From equation (36) we have

$$C_{\text{eff}}(m;m)=\sin^2(\pi m\Delta+\delta)\,C\,(m;m) \quad (39)$$

or if Δ and δ are both small

$$C_{\text{eff}}(m;m)=(\pi m\Delta+\delta)^2\,C\,(m;m). \quad (40)$$

If the transfer function is to have no zeros in the pass band we require that

$$\delta\geq 2\pi\Delta\sin\alpha/\lambda. \quad (41)$$

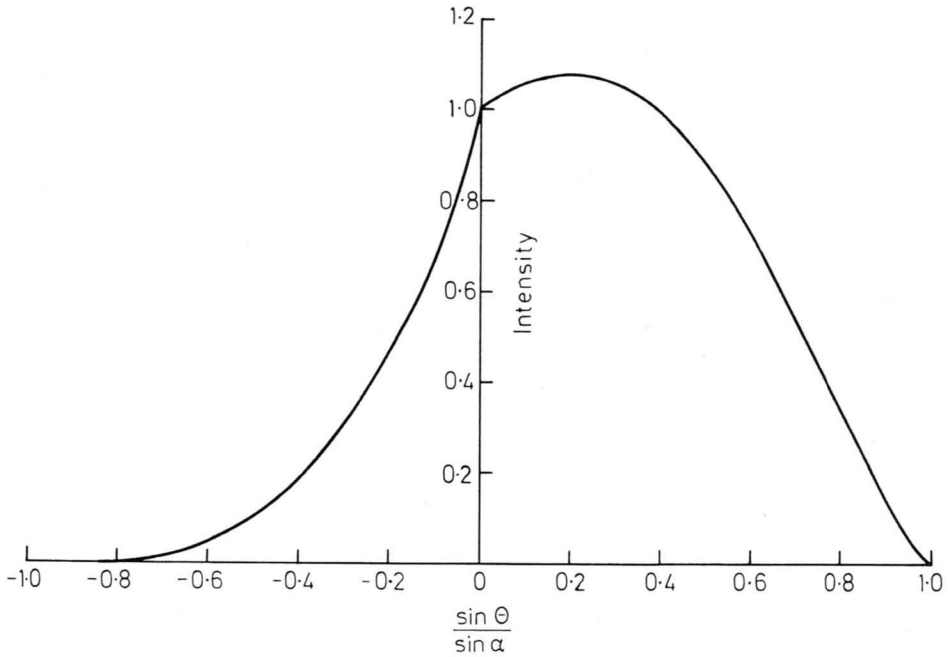

Fig. 12. The signal intensity for a surface at an angle θ, Nomarski DIC with compensator set to just give no zeros in the pass band.

The fractional rate of change of intensity with slope is larger for small δ, so that the maximum differential phase contrast, whilst ensuring no zeros in the transfer function, is obtained when

$$\delta = 2\pi\Delta \sin \alpha/\lambda. \tag{42}$$

Then the transfer function with equal circular pupils is as shown in Fig. 12. It will be noticed that the transfer function is assymmetric, that is positive and negative slopes result in different changes from the indisturbed intensity. For a monotonic phase variation it is possible to get two bright fringes for one sign of phase change and only one dark fringe for the other.

By consideration of equation (9) it is seen that

$$\left.\frac{d\Lambda(\tilde{m})}{d\tilde{m}}\right|_{\tilde{m}\to 0} = \pm\frac{4}{\pi} \tag{43}$$

so that unless $\delta/\pi\Delta$ is such that the zero occurs at a spatial frequency smaller than 2π times the cut-off frequency no brightening of the image occurs at phase gradients but only darkenings, regardless of the sign of the gradient.

If the amplitude of the phase variations is small, say ϵ, δ may be reduced below the value given by equation (41) in order to increase the contrast of the differential phase image, but only by a factor ϵ as then the non-linear components of strength ϵ^2 become appreciable.

6. CONCLUSIONS

Reflection and transmission images have been produced using the split detector technique in a scanning optical microscope. The images are of high quality and resolution, and are free from optical artefacts. The technique has a number of important advantages over the usual Nomarski method of differential interference contrast. The images are produced by pure differential phase contrast, signal level is comparatively high, contrast is controllable electronically, and the full collector aperture may be used to give optimum resolution.

The main differences between the Nomarski method and the split detector technique are thus as follows. Firstly, in the Nomarski method the image is a complicated mixture of different contrast mechanisms, the relative strengths of which can be altered by adjustment of the compensator, whereas using the split detector pure differential phase contrast results. Secondly, the Nomarski method results in an asymmetric response to phase gradients, unlike the split detector method. Thirdly, the split detector method gives no image from a strong point object, unlike the Nomarski technique.

REFERENCES

Barna, A. (1977) Fraunhofer diffraction by semicircular apertures. *J. Opt. Soc. Am.* **67**, 122.

Dekkers, N.H. & de Lang, H. (1974) Differential phase contrast in a STEM. *Optik*, **41**, 452–456.

Dekkers, N.H. & de Lang, H. (1977) A detection method for producing phase and amplitude images simultaneously in a scanning transmission electron microscope. *Philips Tech. Rev.* **37**, 1–9.

Ditkin, V.A. & Prudnikov, A.P. (1965) *Integral Transforms and Operational Calculus*. Pergamon Press, Oxford.

Nomarski, G. (1955) Microinterferometrie differential à ondes polarisées. *J. Phys. Radium*, **16**, 9–135.

Sheppard, C.J.R. (1980a) Scanning optical microscope. *Electronics and Power*, pp. 166–172.

Sheppard, C.J.R. (1980b) Imaging modes of scanning optical microscopy. In: *Scanned Image Microscopy* (Ed. by E. A. Ash), pp. 201–225. Academic Press, London.

Sheppard, C.J.R. & Choudhury, A. (1977) Image formation in the scanning microscope. *Opt. Acta*, **24**, 1051–1073.

Sheppard, C.J.R. & Wilson, T. (1980) Fourier imaging of phase information in scanning and conventional microscopes. *Phil. Trans. Roy. Soc. Lond.* **A295**, 513–536.

Wilson, T. & Sheppard, C.J.R. (1980) Coded apertures and detectors for optical differentiation. *Proc. Soc. Photo-Opt. Instr. Eng.* **232**, 203–209.